PAPER Special Issue on Electromagnetic Theory—Scattering and Diffraction—

A Comparative Study of RCS Predictions of Canonical Rectangular and Circular Cavities with Double-Layer Material Loading

Shoichi KOSHIKAWA†, *Member*, **Dilek ÇOLAK**††, **Ayhan ALTINTAŞ**†††, *Nonmembers*, **Kazuya KOBAYASHI**††††a), *Member, and* **Alexander I. NOSICH**†††††, *Nonmember*

SUMMARY A rigorous radar cross section (RCS) analysis is carried out for two-dimensional rectangular and circular cavities with double-layer material loading by means of the Wiener-Hopf (WH) technique and the Riemann-Hilbert problem (RHP) technique, respectively. Both E and H polarizations are treated. The WH solution for the rectangular cavity and the RHP solution for the circular cavity involve numerical inversion of matrix equations. Since both methods take into account the edge condition explicitly, the convergence of the WH and RHP solutions is rapid and the final results are valid over a broad frequency range. Illustrative numerical examples on the monostatic and bistatic RCS are presented for various physical parameters and the far field scattering characteristics are discussed in detail. It is shown that the double-layer lossy material loading inside the cavities leads to the significant RCS reduction.

key words: *Wiener-Hopf technique, Riemann-Hilbert problem technique, scattering and diffraction, radar cross section, rectangular cavity, circular cavity*

1. Introduction

The analysis of the electromagnetic wave scattering by open cavities is an important subject in radar cross section (RCS) reduction and target identification studies, since these obstacles contribute significantly to the RCS due to the interior irradiation. Cavity structures are encountered in many radar targets such as aircrafts and ships and hence, it is often required to reduce the RCS either by loading the interior of cavities with absorbing materials or by shaping cavities. Some of the cavity diffraction problems have been analyzed thus far using a variety of analytical and numerical methods [1]-[8]. However, it appears that the solutions obtained by these approaches are not uniformly valid for arbitrary cavity dimensions.

The Wiener-Hopf (WH) technique [9]-[11] and the Riemann-Hilbert problem (RHP) technique [12], [13] are established function-theoretic methods for solving scattering and diffraction problems associated with canonical, two-dimensional (2-D) structures. It is well known that the former and latter approaches are suitable for the scattering analysis of 2-D obstacles formed by parallel-plate and circular-arc boundaries, respectively. Both the WH and RHP techniques are mathematically rigorous in the sense that they incorporate the edge condition explicitly into the analysis. There are some recent contributions on the scattering by cavities based on the WH and RHP techniques [14]-[22], in which accurate and reliable results have been obtained over a broad frequency range. It has also been shown in [16]-[22] that the efficient RCS reduction is achieved by loading the interior of cavities with absorbing materials.

Taking into account the above-mentioned analytical advantages of the WH technique for parallel-plate geometries and those of the RHP technique for circular-arc geometries, we have carried out a comparative RCS study in [23] for 2-D rectangular and circular cavities with single-layer material loading by using the WH and RHP techniques, respectively. As a generalization to the cavity configurations treated previously in [23], we shall consider in this paper 2-D rectangular and circular cavities with double-layer material loading, and analyze the plane wave diffraction rigorously using the WH and RHP techniques, respectively. Both E and H polarizations are treated. It is shown via illustrative numerical examples on the monostatic and bistatic RCS that the interior irradiation is significantly reduced over a broad frequency range for cavities with double-layer material loading. In the following, the analysis procedure is presented only for the H-polarized case, but numerical results are given for both polarizations.

The time factor is assumed to be $e^{-i\omega t}$ and suppressed throughout this paper.

Manuscript received February 7, 1997.
Manuscript revised June 7, 1997.

† The author is with Antenna Giken Co., Ltd., Ohmiya-shi, 330 Japan.
†† The author is with the ElectroScience Laboratory, The Ohio State University, Columbus, Ohio 43212, USA.
††† The author is with the Department of Electrical Engineering, Bilkent University, Ankara TR-06533, Turkey.
†††† The author is with the Department of Electrical and Electronic Engineering, Chuo University, Tokyo, 112 Japan.
††††† The author is with the Institute of Radiophysics and Electronics, Ukrainian Academy of Sciences, Kharkov 310085, Ukraine.
a) E-mail: kazuya@kazuya.elect.chuo-u.ac.jp

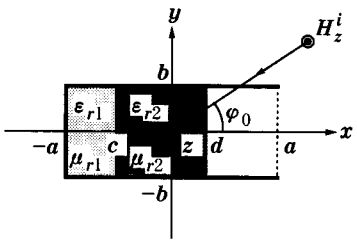

Fig. 1 Geometry of the rectangular cavity $(-a<c<d<a)$.

2. A 2-D Rectangular Cavity: The WH Solution

In this section, we shall consider a 2-D rectangular cavity with double-layer material loading, and analyze the H-polarized plane wave diffraction using the WH technique. The geometry of the problem is shown in Fig. 1, where the cavity plates are perfectly conducting and of zero thickness. The material layers I$(-a<z<c)$ and II$(c<z<d)$ inside the cavity are characterized by the relative permittivity and permeability $(\varepsilon_{rm}, \mu_{rm})$ for $m=1, 2$, respectively. Let the total magnetic field be

$$H_z^t(x, y)=H_z^i(x, y)+H_z(x, y), \tag{1}$$

where $H_z^i(x, y)$ is the incident field defined by

$$H_z^i(x, y)=e^{-ik(x\cos\varphi_0+y\sin\varphi_0)}, \quad 0\leqq\varphi_0\leqq\pi \tag{2}$$

with $k(=\omega\sqrt{\mu_0\varepsilon_0})$ being the free-space wavenumber. For analytical convenience, we introduce a slight loss into the medium as in $k=k_1+ik_2$ with $0<k_2\ll k_1$. The solution for real k is obtained by taking the limit $k_2\to+0$ at the end of analysis.

Let us define the Fourier transform of the scattered field $H_z(x, y)$ with respect to x by

$$\Phi(s, y)=\frac{1}{\sqrt{2\pi}}\int_{-\infty}^{\infty}H_z(x, y)\,e^{isx}dx, \quad s=\sigma+i\tau. \tag{3}$$

In view of the radiation condition, it follows that $\Phi(s, y)$ is regular for $|\tau|<k_2$. Taking the Fourier transform of the 2-D Helmholtz equation and solving the resultant equations, we may derive the scattered field representation in the complex domain. In particular, the field for $y\gtrless\pm b$ is given by

$$\phi(s, y)=\mp[1/2\chi(s)]\{e^{-isa}[U_-(s)\pm V_-(s)]+e^{isa}[U_+(s)\pm V_+(s)]\}e^{\mp\chi(s)(y\mp b)}, \tag{4}$$

where $\chi(s)=\sqrt{s^2-k^2}$ with $\mathrm{Re}\chi(s)>0$, and

$$U_\pm(s)=\Psi'_\pm(s, b)+\Psi'_\pm(s, -b), \tag{5a}$$

$$V_\pm(s)=\Psi'_\pm(s, b)-\Psi'_\pm(s, -b), \tag{5b}$$

$$\Psi'_\pm(s, y)=\Phi'_\pm(s, y)\pm\frac{k\sin\varphi_0 e^{-ik(\pm a\cos\varphi_0+y\sin\varphi_0)}}{\sqrt{2\pi}i(s-k\cos\varphi_0)}, \tag{6}$$

$$\Phi'_\pm(s, y)=\pm\frac{1}{\sqrt{2\pi}}\int_{\pm a}^{\pm\infty}\frac{\partial H_z(x, y)}{\partial y}e^{is(x\mp a)}dx. \tag{7}$$

In (5a), (5b), (6), and (7), the prime denotes differentiation with respect to y.

Applying boundary conditions at the cavity surface and the material interfaces, the problem is formulated in terms of the WH equations satisfied by $U_\pm(s)$ and $V_\pm(s)$. These equations can be solved exactly in a formal sense via the factorization and decomposition procedure with the result that

$$U_\pm(s)=M_\pm(s)\left[\mp\frac{A^u_{1,2}}{\sqrt{b}\,(s-k\cos\varphi_0)}+J^u_{1,2}(s)-\sqrt{b}\,F^u_\pm(s)\right], \tag{8a}$$

$$V_\pm(s)=N_\pm(s)\left[\pm\frac{A^v_{1,2}}{\sqrt{b}\,(s-k\cos\varphi_0)}+J^v_{1,2}(s)-\sqrt{b}\,F^v_\pm(s)\right], \tag{8b}$$

where $M_\pm(s)$ and $N_\pm(s)$ are the split functions defined in [18], and

$$A^u_{1,2}=-\sqrt{\frac{2b}{\pi}}\frac{k\sin\varphi_0 e^{\mp ika\cos\varphi_0}\cos(kb\sin\varphi_0)}{M_\pm(k\cos\varphi_0)}, \tag{9a}$$

$$A^v_{1,2}=-\sqrt{\frac{2b}{\pi}}\frac{ik\sin\varphi_0 e^{\mp ika\cos\varphi_0}\sin(kb\sin\varphi_0)}{N_\pm(k\cos\varphi_0)}, \tag{9b}$$

$$\left.\begin{matrix}J^u_{1,2}(s)\\J^v_{1,2}(s)\end{matrix}\right\}=\frac{1}{\pi i}\int_k^{k+i\infty}\frac{e^{2iwa}}{\chi(w)(w\pm s)}\cdot\left\{\begin{matrix}M_+(w)\,U_\mp(\mp w)\\N_+(w)\,V_\mp(\mp w)\end{matrix}\right\}dw, \tag{10}$$

$$F^u_\pm(s)=\sum_{n=2}^{\infty}\left\{\begin{matrix}\chi_{2n-3}\\1\end{matrix}\right\}\frac{f_n p_n u_n^\pm}{b(s\pm ik_{2n-3})}, \tag{11a}$$

$$F^v_\pm(s)=\sum_{n=1}^{\infty}\left\{\begin{matrix}\chi_{2n-2}\\1\end{matrix}\right\}\frac{\nu_{2n-2}g_n q_n v_n^\pm}{b(s\pm ik_{2n-2})}, \tag{11b}$$

$$v_0=1/2;\ v_n=1 \quad \text{for} \quad n\geqq1, \tag{12}$$

$$\chi_n=\frac{e^{-2\kappa_n(a-d)}[\sigma_{1n}e^{-2K_{2n}(d-c)}-\sigma_{2n}]}{1-\sigma_{1n}\sigma_{2n}e^{-2K_{2n}(d-c)}}, \tag{13}$$

$$\sigma_{1n}=\frac{(\varepsilon_{r2}/\varepsilon_{r1})K_{1n}-\tau_nK_{2n}}{(\varepsilon_{r2}/\varepsilon_{r1})K_{1n}+\tau_nK_{2n}}, \quad \tau_n=\frac{1-e^{-2K_{1n}(c+a)}}{1+e^{-2K_{1n}(c+a)}}, \tag{14a}$$

$$\sigma_{2n}=\frac{\varepsilon_{r2}\chi_n-K_{2n}}{\varepsilon_{r2}\chi_n+K_{2n}}, \tag{14b}$$

$$f_1=(bix_0)^{-1};\ f_n=(bix_{2n-3})^{-1} \quad \text{for} \quad n\geqq2, \tag{15a}$$

$$g_1=(bix_0)^{-1};\ g_n=(bix_{2n-2})^{-1} \quad \text{for} \quad n\geqq 2, \tag{15b}$$

$$p_1=\sqrt{b}\,M_+(ix_0);\ p_n=\sqrt{b}\,M_+(ix_{2n-3}) \quad \text{for} \quad n\geqq 2, \tag{16a}$$

$$q_1=\sqrt{b}\,N_+(ix_0);\ q_n=\sqrt{b}\,N_+(ix_{2n-2}) \quad \text{for} \quad n\geqq 2, \tag{16b}$$

$$u_1^{\pm}=U_{\pm}(\pm ix_0);\ u_n^{\pm}=U_{\pm}(\pm ix_{2n-3}) \quad \text{for} \quad n\geqq 2, \tag{17a}$$

$$v_1^{\pm}=V_{\pm}(\pm ix_0);\ v_n^{\pm}=V_{\pm}(\pm ix_{2n-2}) \quad \text{for} \quad n\geqq 2, \tag{17b}$$

$$x_0=-ik;\ x_n=\sqrt{(n\pi/2b)^2-k^2} \quad \text{for} \quad n\geqq 1, \tag{18a}$$

$$K_{m0}=-ik_{rm};\ K_{mn}=\sqrt{(n\pi/2b)^2-k_{rm}^2} \quad \text{for} \quad n\geqq 1, \tag{18b}$$

$$k_{rm}=\sqrt{\mu_{rm}\varepsilon_{rm}}\,k. \tag{19}$$

We may apply the method established in [17], [22] to derive approximate expressions of the infinite series $F_{\pm}^{u}(s)$, $F_{\pm}^{v}(s)$ and the branch-cut integrals $J_{1,2}^{u}(s)$, $J_{1,2}^{v}(s)$ defined by (10), (11a), and (11b). In particular, $J_{1,2}^{u}(s)$ can be expanded asymptotically as

$$J_{1,2}^{u}(s)\sim \sqrt{b}\,f_1p_1\left\{\left[u_1^{\mp}+\frac{2A_{2,1}\cos(kb\sin\varphi_0)}{kb(1\pm\cos\varphi_0)}\right]\xi(\pm s)+\frac{2aA_{2,1}}{b}\cos(kb\sin\varphi_0)\,\eta(\pm s,\ \pm k\cos\varphi_0)\right\} \tag{20}$$

for large $|k|a$, and approximate expressions of $F_{\pm}^{u}(s)$ are derived by using the edge condition as

$$F_{\pm}^{u}(s)\approx\sum_{n=2}^{N}\begin{Bmatrix}\chi_{2n-3}\\ 1\end{Bmatrix}\frac{f_np_nu_n^{\pm}}{b(s\pm ix_{2n-3})}+C_{1,2}^{u}\sum_{n=N+1}^{\infty}\begin{Bmatrix}\chi_{2n-3}\\ 1\end{Bmatrix}\frac{(bx_{2n-3})^{-c_{1,2}}}{b(s\pm ix_{2n-3})} \tag{21}$$

for large N with $c_1=7/6$ and $c_2=1$, where $C_{1,2}^{u}$ are unknown constants, and

$$\xi(s)=\frac{\sqrt{ka}\,e^{i(2ka-3\pi/4)}}{\pi}\Gamma_1[1/2,\ -2i(s+k)a], \tag{22}$$

$$\eta(s_1,\ s_2)=\frac{\xi(s_1)-\xi(s_2)}{(s_1-s_2)a}. \tag{23}$$

In (22), $\Gamma_1(\cdot,\cdot)$ is the generalized gamma function defined in [24].

Using (20) and (21), we can derive approximate expressions of (8a), which are valid for the cavity depth $2a$ greater than the wavelength. The unknowns $u_n^{\pm}$ for $n=1, 2, 3, \cdots, N$ and $C_{1,2}^{u}$ are determined by solving an appropriate matrix equation numerically [22]. We have verified from the detailed numerical experimentation that sufficiently accurate results are obtained by choosing $N\geqq 2kb/\pi$. Approximate expressions of (8b) are derived following the same procedure as above. The scattered field in the real space for $|y|>b$ is evaluated asymptotically by taking the inverse Fourier transform of (4) and applying the saddle point method. The solution obtained in this section is a special case of the results presented in our recent paper [20].

3. A 2-D Circular Cavity: The RHP Solution

We now consider a 2-D circular cavity with double-layer material loading, illuminated by an H-polarized plane wave, as shown in Fig. 2, where the cavity wall is infinitely thin and perfectly conducting. The material layers I ($d<r<a$) and II ($c<r<d$) inside the cavity are characterized by the relative permittivity and permeability (ε_{rm}, μ_{rm}) for $m=1, 2$, respectively. Let the total magnetic field be

$$H_z^t(x,\ y)=\begin{cases}H_z^i(x,\ y)+H_z(x,\ y), & r>a,\\ H_z(x,\ y), & r<a\end{cases} \tag{24}$$

with H_z^i being the incident field defined by (2). The scattered field H_z in (24) can be expanded as

$$H_z(r,\ \varphi)=\sum_{n=-\infty}^{\infty}f_n(r)\,e^{in\varphi} \tag{25}$$

in cylindrical coordinates, where

$$f_n(r)=\begin{cases}A_nH_n^{(1)}(kr), & r>a,\\ B_nJ_n(k_{r1}r)+C_nH_n^{(1)}(k_{r1}r), & d<r<a,\\ D_nJ_n(k_{r2}r)+E_nH_n^{(1)}(k_{r2}r), & c<r<d,\\ F_nJ_n(kr), & r<c\end{cases} \tag{26}$$

with $H_n^{(1)}(\cdot)$ and $J_n(\cdot)$ being the Hankel and Bessel functions, respectively.

Applying boundary conditions for H_z^t and $\partial H_z^t/\partial r$ at $r=c$, d to eliminate B_n, C_n, D_n, E_n, F_n in (26) and taking into account the boundary condition at $r=$

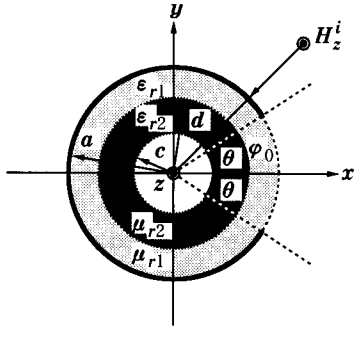

Fig. 2 Geometry of the circular cavity ($0<c<d<a$).

a, we arrive at the dual series equations (DSE) as in

$$\sum_{n=-\infty}^{\infty} x_n e^{in\varphi}=0, \quad \theta<|\varphi|\leqq\pi, \tag{27a}$$

$$\sum_{n=-\infty}^{\infty} x_n\gamma_n e^{in\varphi}=-\sum_{n=-\infty}^{\infty} d_n e^{in\varphi}, \quad |\varphi|<\theta, \tag{27b}$$

where

$$x_n=A_nH_n^{(1)\prime}(ka)+(-i)^nJ_n'(ka)\,e^{-in\varphi_0}, \tag{28}$$

$$d_n=-\frac{2(-i)^{n+1}e^{-in\varphi_0}}{\pi kaH_n^{(1)\prime}(ka)}, \tag{29}$$

$$\gamma_n=\frac{H_n^{(1)}(ka)}{H_n^{(1)\prime}(ka)} -\eta_{r1}\frac{\xi_nJ_n(k_{r1}a)-\zeta_nH_n^{(1)}(k_{r1}a)}{\xi_nJ_n'(k_{r1}a)-\zeta_nH_n^{(1)\prime}(k_{r1}a)} \tag{30}$$

with

$$\xi_n=\alpha_{1n}\beta_{1n}-\alpha_{2n}\beta_{2n}, \quad \zeta_n=\alpha_{3n}\beta_{1n}-\alpha_{4n}\beta_{2n}, \tag{31}$$

$$\alpha_{1n}=H_n^{(1)}(k_{r1}d)\,J_n'(k_{r2}d) -\eta_sH_n^{(1)\prime}(k_{r1}d)\,J_n(k_{r2}d), \tag{32a}$$

$$\alpha_{2n}=H_n^{(1)}(k_{r1}d)\,H_n^{(1)\prime}(k_{r2}d) -\eta_sH_n^{(1)\prime}(k_{r1}d)\,H_n^{(1)}(k_{r2}d), \tag{32b}$$

$$\alpha_{3n}=J_n(k_{r1}d)\,J_n'(k_{r2}d)-\eta_sJ_n'(k_{r1}d)\,J_n(k_{r2}d), \tag{33a}$$

$$\alpha_{4n}=J_n(k_{r1}d)\,H_n^{(1)\prime}(k_{r2}d) -\eta_sJ_n'(k_{r1}d)\,H_n^{(1)}(k_{r2}d), \tag{33b}$$

$$\beta_{1n}=H_n^{(1)}(k_{r2}c)\,J_n'(kc)-\eta_{r2}H_n^{(1)\prime}(k_{r2}c)\,J_n(kc), \tag{34a}$$

$$\beta_{2n}=J_n(k_{r2}c)\,J_n'(kc)-\eta_{r2}J_n'(k_{r2}c)\,J_n(kc), \tag{34b}$$

$$\eta_{rm}=\sqrt{\varepsilon_{rm}/\mu_{rm}}, \quad \eta_s=\eta_{r1}/\eta_{r2}. \tag{35}$$

In the above, the prime on $H_n^{(1)}(\cdot)$ and $J_n(\cdot)$ implies differentiation with respect to the argument. It can be shown that γ_n given by (30) behaves like $-|n|^{-1}\cdot ka(\varepsilon_{r1}+1)^{-1}$ as $|n|\to\infty$. Taking into account this asymptotic behavior, we can rearrange (27b) so that its left-hand side contains the weight factor $|n|$. We now introduce the functions $X^{\pm}(z)$ of a complex variable $z=|z|e^{i\arg z}$ as $X^{\pm}(z)=\sum_{n=1}^{\infty} nx_{\pm n}z^{\pm n}$ with plus and minus signs corresponding to $|z|\leqq 1$ and $|z|\geqq 1$, respectively. Then such a DSE can be reduced to the Riemann-Hilbert functional equation satisfied by the limiting values of $X^{\pm}(z)$ on the unit circle $|z|=1$. Provided that the right-hand side is a known function, this functional equation can be solved exactly based on the theory of Cauchy's integrals [12]. In our case, the right-hand side of such a DSE depends on the coefficients x_n. Application of the RHP technique now results in the matrix equation of the Fredholm second kind as

$$y_m=\sum_{n=-\infty}^{\infty} K_{mn}y_n+L_m, \quad m=0,\ \pm1,\ \pm2,\ \cdots, \tag{36}$$

where

$$K_{mn}=P_nT_{mn}, \tag{37}$$

$$L_m=-ka(\varepsilon_{r1}+1)\sum_{n=-\infty}^{\infty}\frac{d_n}{\gamma_n}T_{mn}, \tag{38}$$

$$P_n=\frac{ka(\varepsilon_{r1}+1)}{\gamma_n}+|n|, \tag{39}$$

$$y_n=x_n\gamma_n+d_n, \tag{40}$$

$$T_{mn}=(-1)^{m+n}\begin{cases} Q_{mn}(-\cos\theta), & m\neq 0,\\ Q_{n0}(-\cos\theta), & m=0,\ n\neq 0,\\ -\ln[(1-\cos\theta)/2], & m=n=0, \end{cases} \tag{41}$$

and $Q_{mn}(\cdot)$ is defined in [16] using the Legendre polynomials.

We can show by taking into account the asymptotic behavior of K_{mn} for $|m|$, $|n|\to\infty$ that $\sum_{m,n=-\infty}^{\infty}|K_{mn}|^2<\infty$ and $\sum_{m=-\infty}^{\infty}|L_m|^2<\infty$. Hence it follows by application of the Fredholm theorems that the solution of (36) does exist and is unique. In addition, the solution can be approximated with any desired accuracy by means of truncation of the matrix equation. Practically, after separating the matrix into even and odd parts, $|k_{r1}|a+10$ equations are sufficient to obtain the far field quantities within the 0.1% accuracy. Unlike the conventional moment method solutions, no numerical integrations are required for computing the matrix elements and hence, the present solution is efficient in the computational sense. It should be noted that, in view of the asymptotic behavior $P_n=O(k^2a^2\cdot|n|^{-1})$ for small ka, the procedure described above is equivalent to the analytical inversion of the static part of the DSE given by (27a) and (27b).

4. Numerical Results and Discussion

In this section, we shall present numerical examples on the RCS to discuss the far field scattering characteristics of the rectangular and circular cavities in detail for both E and H polarizations. In order to have a better ground for comparison, we take a square-shaped cavity ($a=b$ in Fig. 1) and a three-quarter circular cavity ($\theta=45°$ in Fig. 2). In numerical computation, we have considered the double-layer material with $\varepsilon_{r1}=1.6+i0.9$, $\varepsilon_{r2}=1.4+i0.35$, $\mu_{r1}=\mu_{r2}=1.0$ for the rectangular cavity and $\varepsilon_{r1}=1.4+i0.35$, $\varepsilon_{r2}=1.6+i0.9$, $\mu_{r1}=\mu_{r2}=1.0$ for the circular cavity. These material constants have been taken from the existing absorber known as Emerson & Cuming AN-73 [25]. It is to be noted here that we have chosen the material constants such that

$(\varepsilon_{r1}, \mu_{r1})$ and $(\varepsilon_{r2}, \mu_{r2})$ for the rectangular cavity are equal to $(\varepsilon_{r2}, \mu_{r2})$ and $(\varepsilon_{r1}, \mu_{r1})$ for the circular cavity, respectively, since the incident wave first impinges the layer II $(c<z<d)$ for the rectangular case and the layer I $(d<r<a)$ for the circular case. The thickness of each layer is chosen such that $c+a=d-c$ $(=t/2)$ for the rectangular cavity and $a-d=d-c(=t/2)$ for the circular cavity. The total thickness of the double-layer material has been taken as $kt=3.84$ for the rectangular cavity and hence, the corresponding thickness for the circular cavity has been chosen as $kt=1.92$. This thickness is an optimum value from the viewpoint of RCS reduction, which has been determined by numerical experimentation so that the reflected power becomes small when the plane wave is normally incident on the double-layer material coated on a perfectly conducting plate. This choice of parameters for the material constants and the material thickness may enable comparison on the scattering characteristics between rectangular and circular cavities. The RCS data for empty cavities have also been plotted in order to investigate the effect of material loading.

Figures 3 and 4 show the frequency dependences of the monostatic RCS for rectangular and circular cavities, respectively, where the incidence angle is $\varphi_0=0°$ for both geometries. For empty cavities, we see that the average RCS level becomes large with an increase of the normalized frequency kb in Fig. 3 and ka in Fig. 4. It is also found that the empty circular cavity exhibits stronger resonances than the empty rectangular cavity. This is perhaps due to the whispering-gallery behavior of the higher order natural modes in the circular cavity, which does not appear in the rectangular case. We also notice that the lossy material loading inside the cavities leads to the reduction of the average RCS level over the whole frequency range

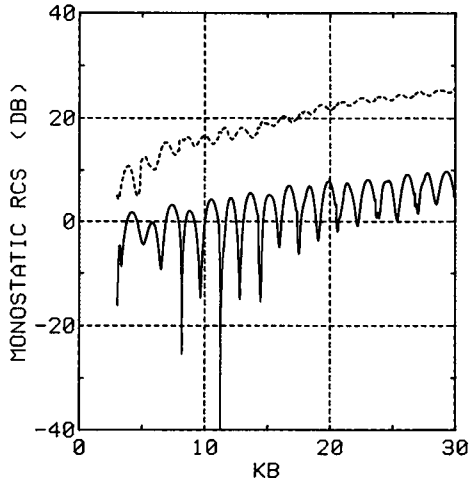

(a) E polarization.

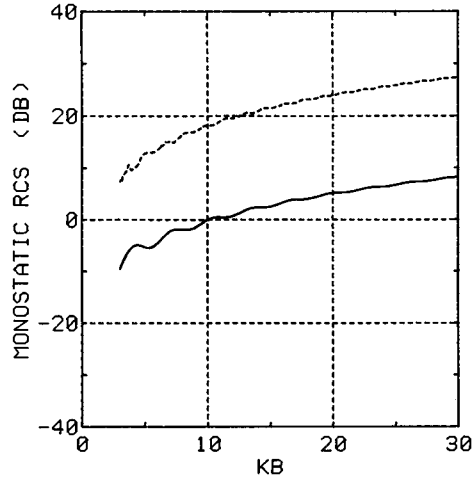

(b) H polarization.

Fig. 3 Monostatic RCS versus normalized frequency kb of a rectangular cavity for $\varphi_0=0°$, $a/b=1.0$.
-----: empty; ———: double-layer loading with $\varepsilon_{r1}=1.6+i0.9$, $\varepsilon_{r2}=1.4+i0.35$, $\mu_{r1}=\mu_{r2}=1.0$, $kt=3.84$.

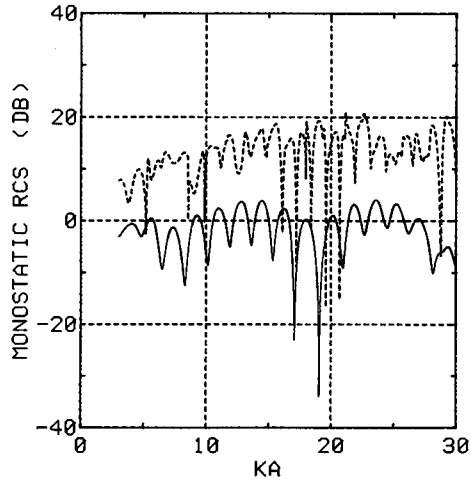

(a) E polarization.

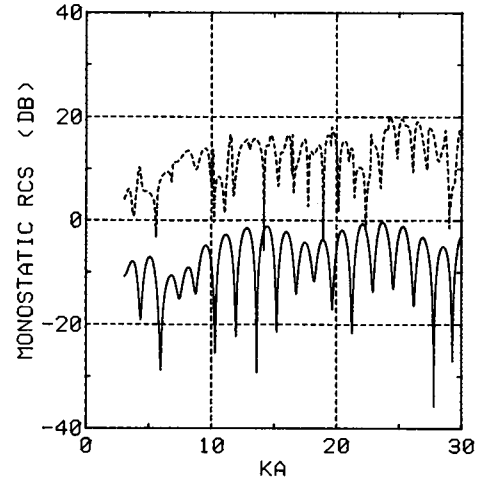

(b) H polarization.

Fig. 4 Monostatic RCS versus normalized frequency ka of a circular cavity for $\varphi_0=0°$, $\theta=45°$.
-----: empty; ———: double-layer loading with $\varepsilon_{r1}=1.4+i0.35$, $\varepsilon_{r2}=1.6+i0.9$, $\mu_{r1}=\mu_{r2}=1.0$, $kt=1.92$.

shown in the figures. Comparing the characteristics for loaded rectangular cavities between E and H polarizations, we observe sharp oscillations due to the waveguide resonances in the E-polarized case, whereas these resonance phenomena are not clearly seen in the H-polarized case. For circular cavities, we observe strong oscillations in both empty and loaded cases, and the RCS characteristics for both polarizations exhibit similar features. Sharp minima and maxima in the circular case correspond to the natural resonances of the cavity, shifted from the zeros of $J_n(ka)$ and $J_n'(ka)$ due to the free-space leakage and the material loading.

We now present the monostatic RCS as a function of incidence angle φ_0 in Figs. 5 and 6 for rectangular cavities, and in Figs. 7 and 8 for circular cavities, where the cavity dimension is chosen as $ka=kb=3.14$, 31.4. Comparing the results for empty and loaded cavities, the RCS is reduced for loaded cavities in the region where the cavity aperture opening is visible from the incident direction. In particular, the RCS reduction is significant over $0°<\varphi_0<30°$. Shown in Figs. 9 and 10 and in Figs. 11 and 12 are the bistatic RCS as a function of observation angle φ for rectangular and circular cavities, respectively, where the incidence angle is fixed as $\varphi_0=45°$ and the cavity dimensions are the same as in Figs. 5-8. It is seen that in all numerical examples, the bistatic RCS has the largest values along the incident shadow boundary at $\varphi=-135°$ and these shadow lobes become sharper and narrower at higher frequencies, as expected. Comparing the RCS characteristics between empty and loaded cavities, we also notice that the RCS is reduced for the loaded case over the region where the cavity aperture is visible from the observation point, and that the RCS reduction is noticeable for $|\varphi|<60°$. This feature becomes more pronounced for larger cavities.

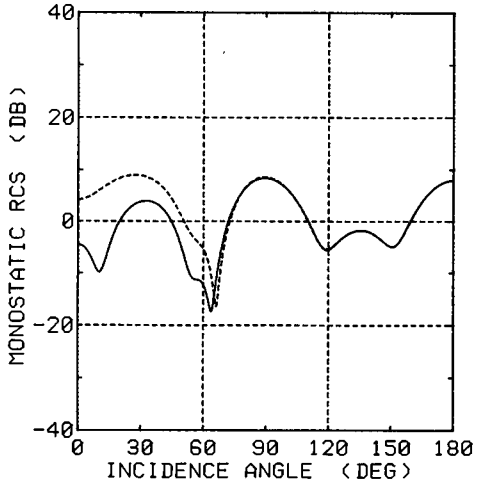

(a) $kb=3.14$.

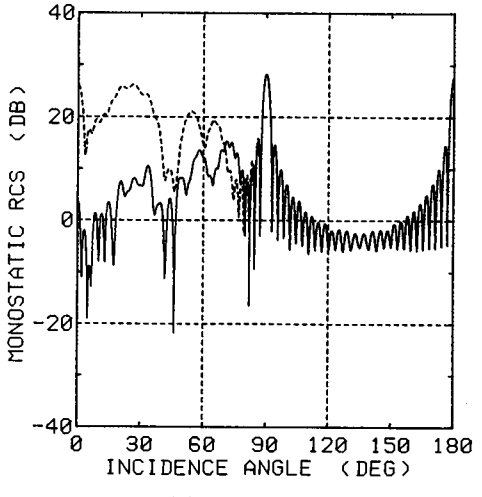

(b) $kb=31.4$.

Fig. 5 Monostatic RCS versus incidence angle φ_0 of a rectangular cavity for E polarization, $a/b=1.0$.
-----: empty; ———: double-layer loading with $\varepsilon_{r1}=1.6+i0.9$, $\varepsilon_{r2}=1.4+i0.35$, $\mu_{r1}=\mu_{r2}=1.0$, $kt=3.84$.

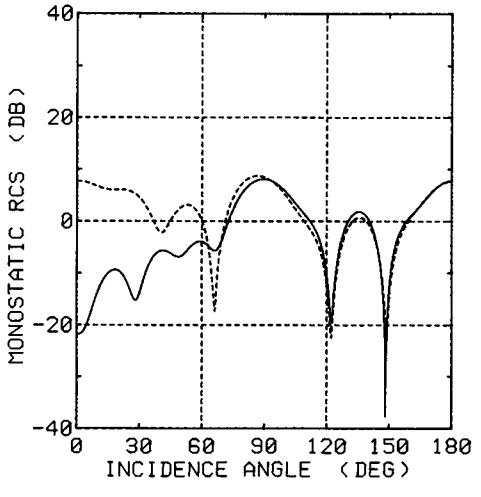

(a) $kb=3.14$.

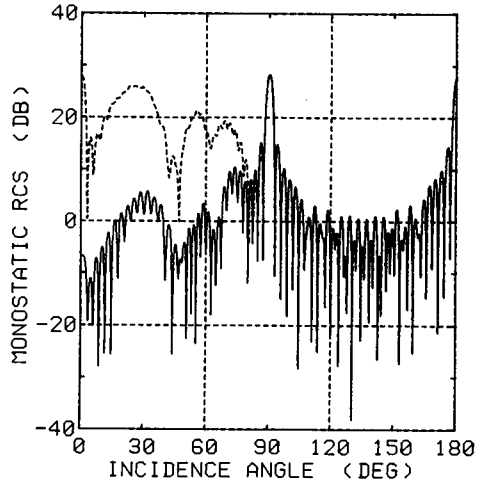

(b) $kb=31.4$.

Fig. 6 Monostatic RCS versus incidence angle φ_0 of a rectangular cavity for H polarization, $a/b=1.0$. Other particulars are the same as in Fig. 5.

5. Conclusions

In this paper, we have considered 2-D rectangular and circular cavities with double-layer material loading, and analyzed rigorously the plane wave diffraction by using the WH and RHP techniques, respectively. Both E and H polarizations have been treated. Illustrative numerical examples on the monostatic and bistatic RCS have been presented, and the far field scattering characteristics of the cavities have been discussed in detail. As a result, it has been clarified that the double-layer material loading is very effective over a broad frequency range in reducing the monostatic RCS when the cavities are illuminated towards their apertures. However, this reduction becomes weaker in the case of the bistatic RCS if the observation direction is away from the aperture direction. It should be emphasized that the WH and RHP solutions obtained in this paper are based on rigorous techniques and are valid for arbitrary cavity dimensions. Since the accuracy of the solutions is in the digital precision of a computer, our results may serve as a reference data for validating other approaches.

Acknowledgments

This work was supported in part by the 1997 Chuo University Special Research Grant and by the Institute of Science and Engineering, Chuo University.

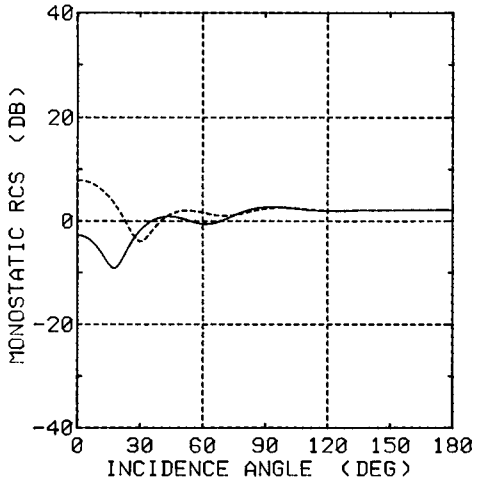

(a) $ka=3.14$.

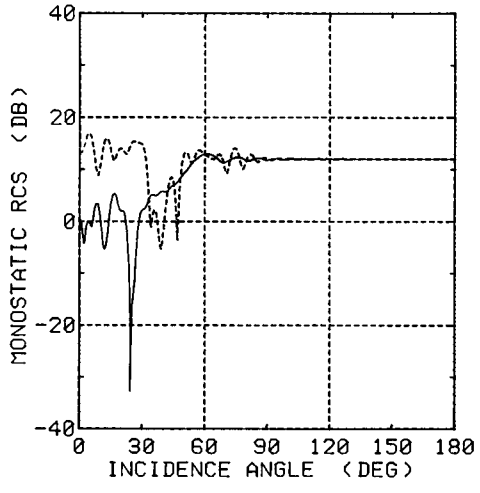

(b) $ka=31.4$.

Fig. 7 Monostatic RCS versus incidence angle φ_0 of a circular cavity for E polarization, $\theta=45°$.
-----: empty; ———: double-layer loading with $\varepsilon_{r1}=1.4+i0.35$, $\varepsilon_{r2}=1.6+i0.9$, $\mu_{r1}=\mu_{r2}=1.0$, $kt=1.92$.

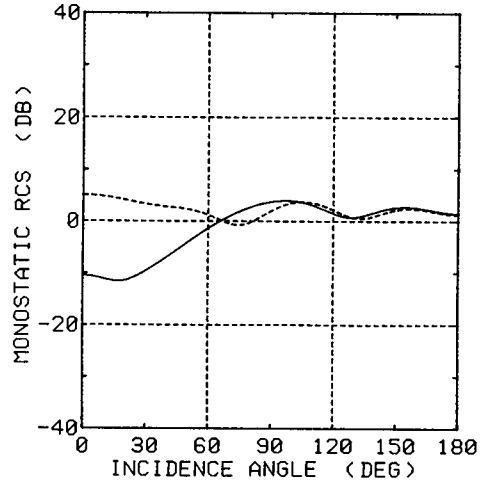

(a) $ka=3.14$.

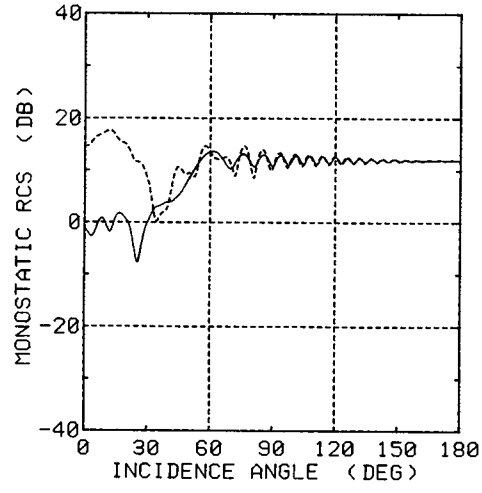

(b) $ka=31.4$.

Fig. 8 Monostatic RCS versus incidence angle φ_0 of a circular cavity for H polarization, $\theta=45°$. Other particulars are the same as in Fig. 7.

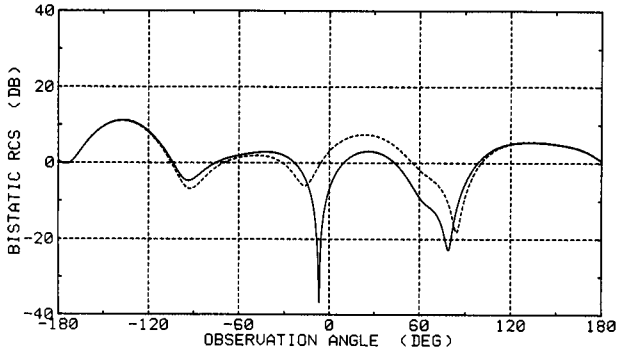

(a) $kb=3.14$.

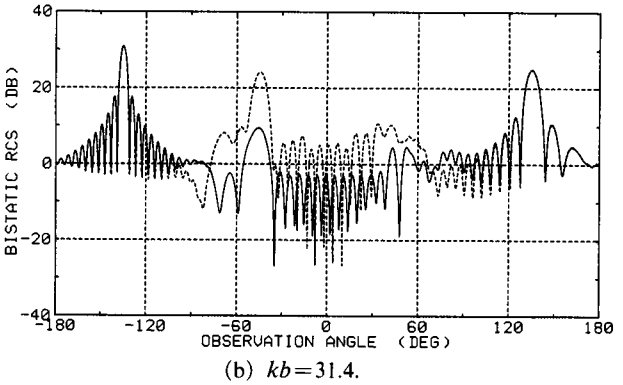

(b) $kb=31.4$.

Fig. 9 Bistatic RCS versus observation angle φ of a rectangular cavity for E polarization, $\varphi_0=45°$, $a/b=1.0$.
----: empty; ———: double-layer loading with $\varepsilon_{r1}=1.6+i0.9$, $\varepsilon_{r2}=1.4+i0.35$, $\mu_{r1}=\mu_{r2}=1.0$, $kt=3.84$.

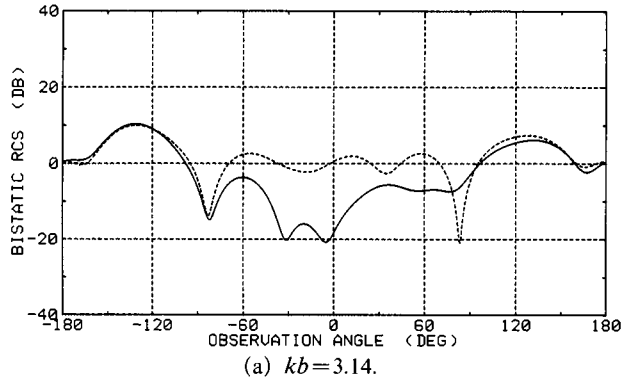

(a) $kb=3.14$.

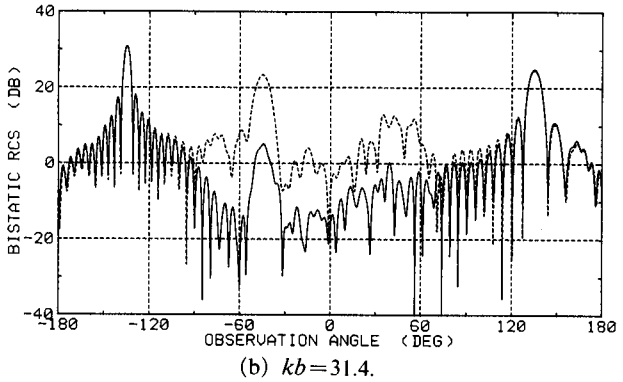

(b) $kb=31.4$.

Fig. 10 Bistatic RCS versus observation angle φ of a rectangular cavity for H polarization, $\varphi_0=45.0°$, $a/b=1.0$. Other particulars are the same as in Fig. 9.

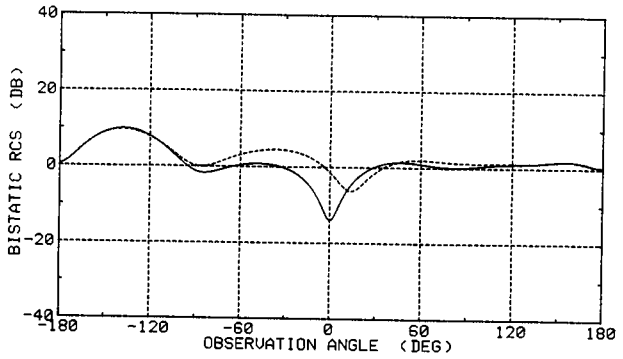

(a) $ka=3.14$.

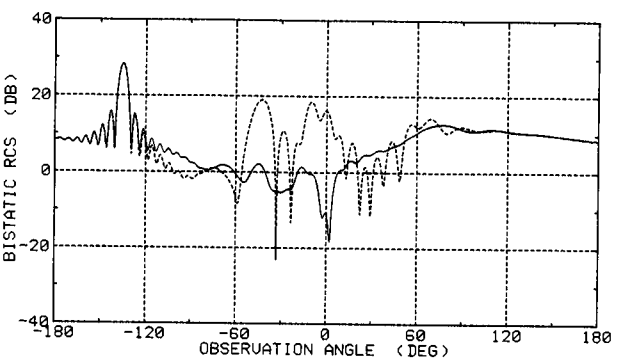

(b) $ka=31.4$.

Fig. 11 Bistatic RCS versus observation angle φ of a circular cavity for E polarization, $\varphi_0=45°$, $\theta=45°$.
----: empty; ———: double-layer loading with $\varepsilon_{r1}=1.4+i0.35$, $\varepsilon_{r2}=1.6+i0.9$, $\mu_{r1}=\mu_{r2}=1.0$, $kt=1.92$.

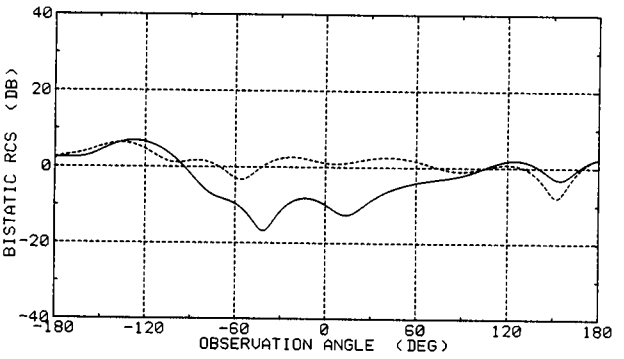

(a) $ka=3.14$.

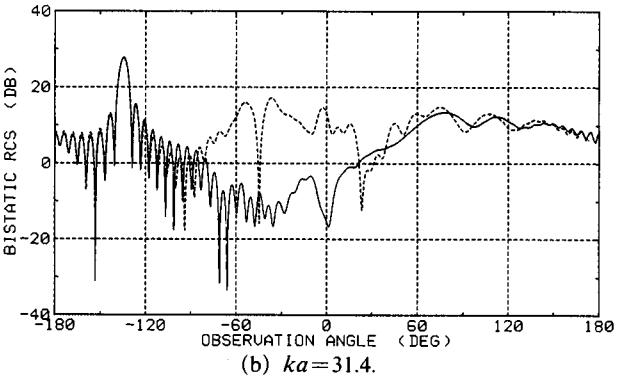

(b) $ka=31.4$.

Fig. 12 Bistatic RCS versus observation angle φ of a circular cavity for H polarization, $\varphi_0=45°$, $\theta=45°$. Other particulars are the same as in Fig. 11.

References

[1] C. S. Lee and S.-W. Lee, "RCS of a coated circular waveguide terminated by a perfect conductor," IEEE Trans. Antennas & Propag., vol. 35, no. 4, pp. 391-398, April 1987.

[2] A. Altintaş, P. H. Pathak, and M. C. Liang, "A selective modal scheme for the analysis of EM coupling into or radiation from large open-ended waveguides," IEEE Trans. Antennas & Propag., vol. 36, no. 1, pp. 84-96, Jan. 1988.

[3] J. R. Mautz and R. F. Harrington, "EM penetration into a conducting circular cylinder through a narrow slot, TM case," J. Electromagn. Waves Appl., vol. 2, no. 3/4, pp. 269-293, 1988.

[4] H. Ling, R.-C. Chou, and S.-W. Lee, "Shooting and bouncing rays: Calculating the RCS of an arbitrary shaped cavity," IEEE Trans. Antennas & Propag., vol. 37, no. 2, pp. 194-205, Feb. 1989.

[5] P. H. Pathak and R. J. Burkholder, "Modal, ray, and beam techniques for analyzing the EM scattering by open-ended waveguide cavities," IEEE Trans. Antennas & Propag., vol. 37, no. 5, pp. 635-647, May 1989.

[6] L. B. Felsen and G. Vecchi, "Wave scattering from slit coupled cylindrical cavities with interior loading: Part II —Resonant mode expansion," IEEE Trans. Antennas & Propag., vol. 39, no. 8, pp. 1085-1097, Aug. 1991.

[7] P. M. Goggans and T. H. Shumpert, "Backscatter RCS for TE and TM excitations of dielectric-filled cavity-backed apertures in two-dimensional bodies," IEEE Trans. Antennas & Propag., vol. 39, no. 8, pp. 1224-1227, Aug. 1991.

[8] A. El-Hajj, K. Y. Kabalan, and R. F. Harrington, "Characteristic mode of a slot in a conducting cylinder and their use for penetration and scattering, TE case," IEEE Trans. Antennas & Propag., vol. 40, no. 2, pp. 156-161, Feb. 1992.

[9] B. Noble, "Methods Based on the Wiener-Hopf Technique for the Solution of Partial Differential Equations," Pergamon Press, London, 1958.

[10] R. Mittra and S.-W. Lee, "Analytical Techniques in the Theory of Guided Waves," Macmillan, New York, 1971.

[11] K. Kobayashi, "The Wiener-Hopf technique with applications to scattering and diffraction problems," A Course of Applied Mathematics, Chap. 9, ed., K. Horiuchi, Corona Publishing, Tokyo, 1989.

[12] F. D. Gakhov, "Boundary Value Problems," Pergamon Press, London, 1966.

[13] A. I. Nosich, "Green's function-dual series approach in wave scattering by combined resonant scatterers," Analytical and Numerical Methods in Electromagnetic Wave Theory, Chap. 9, eds., M. Hashimoto, M. Idemen, and O. A. Tretyakov, Science House, Tokyo, 1993.

[14] W. A. Johnson and R. W. Ziolkowski, "Scattering of an H-polarized plane wave from an axially slotted infinite cylinder: A dual series approach," Radio Sci., vol. 19, no. 1, pp. 275-291, Jan.-Feb. 1984.

[15] R. W. Ziolkowski and J. B. Grant, "Scattering from cavity-backed apertures: The generalized dual series solution of the concentrically loaded E-pol slit cylinder problem," IEEE Trans. Antennas & Propag., vol. 35, no. 5, pp. 504-528, May 1987.

[16] D. Çolak, A. I. Nosich, and A. Altintaş, "Radar cross-section study of cylindrical cavity-backed apertures with outer or inner material coating: The case of E-polarization," IEEE Trans. Antennas & Propag., vol. 41, no. 11, pp. 1551-1559, Nov. 1993.

[17] K. Kobayashi, S. Koshikawa, and A. Sawai, "Diffraction by a parallel-plate waveguide cavity with dielectric/ferrite loading: Part I—The case of E polarization," Progress in Electromagnetics Research, PIER 8, ed., J. A. Kong, Chap. IX, EMW Publishing, Cambridge, 1994.

[18] S. Koshikawa and K. Kobayashi, "Diffraction by a parallel-plate waveguide cavity with dielectric/ferrite loading: Part II—The case of H polarization," Progress in Electromagnetics Research, PIER 8, ed., J. A. Kong, Chap. X, EMW Publishing, Cambridge, 1994.

[19] S. Koshikawa and K. Kobayashi, "Wiener-Hopf analysis of the diffraction by a parallel-plate waveguide cavity with partial material loading," IEICE Trans. Electron., vol. E77-C, no. 6, pp. 975-985, June 1994.

[20] S. Koshikawa T. Momose, and K. Kobayashi, "RCS of a parallel-plate waveguide cavity with three-layer material loading," IEICE Trans. Electron., vol. E77-C, no. 9, pp. 1514-1521, Sept. 1994.

[21] D. Çolak, A. I. Nosich, and A. Altintaş, "Radar cross-section study of cylindrical cavity-backed apertures with outer or inner material coating: The case of H-polarization," IEEE Trans. Antennas & Propag., vol. 43, no. 5, pp. 440-447, May 1995.

[22] K. Kobayashi and S. Koshikawa, "Wiener-Hopf analysis of the radar cross section of parallel-plate waveguide cavities," Tech. Rep., no. KK96-3-8, Chuo Univ., March 1996.

[23] K. Kobayashi and A. I. Nosich, "RCS analysis of canonical, two-dimensional material-loaded cavities with rectangular and circular cross sections," Ann. Telecomm., vol. 50, no. 5-6, pp. 517-522, May-June 1995.

[24] K. Kobayashi, "On generalized Gamma functions occurring in diffraction theory," J. Phys. Soc. Japan, vol. 60, no. 5, pp. 1501-1512, May 1991.

[25] S. -W. Lee and H. Ling, "Data book for cavity RCS: Version 1," Tech. Rep., no. SWL 89-1, Univ. Illinois, Urbana, Jan. 1989.

Shoichi Koshikawa was born in Chiba, Japan, on April 15, 1967. He received the B.S., M.S., and Ph.D. degrees in electrical engineering from Chuo University, Tokyo, Japan, in 1991, 1993, and 1996, respectively. He joined Antenna Giken Co., Ltd. in April 1996, where he is currently working on microwave and millimeter-wave applications. He received the Young Scientist Paper Award of the 5-th International Conference on Mathematical Methods in Electromagnetic Theory (MMET'94). Dr. Koshikawa is a member of the Institute of Electrical Engineers (IEE) of Japan.

Dilek Çolak was born in Aksehir, Turkey, in 1970. She received her B.S. and M.S. degrees in electrical engineering from Bilkent University, Ankara, Turkey, in 1991 and 1993, respectively. She is currently a graduate research associate at the ElectroScience Labarotary, The Ohio State University, working toward the Ph. D. degree. Her research interests include analytical and numerical solutions of electromagnetic scattering problems, radar cross section and antennas. She was one of the recipients of the Young Scientist Award of the International Union of Radio Science (URSI) at the 24th General Assembly in 1993.

Ayhan Altintaş was born on March 29, 1958 in Turkey. He received his B.S. and M.S. degrees from the Middle East Technical University (METU), Ankara, Turkey, in 1979 and 1981, respectively, and the Ph.D. degree from The Ohio State University, Columbus, Ohio, USA in 1986, all in electrical engineering. From 1981 to 1987, he was with the Electro-Science Laboratory, The Ohio State University. Afterward, he spent one year at the Optical Sciences Center of The Australian National University, Canberra, Australia. Currently, he is Professor of Electrical Engineering at Bilkent University, Ankara, Turkey. His research interests are in electromagnetic radiation and scattering, microwaves, fiber optics, and integrated optics. Dr. Altintaş is a member of Sigma Xi and Phi Kappa Phi. He served as the Chairman of IEEE Turkey Section for the terms 1991-1993 and 1995-1997. He is the recipient of the ElectroScience Laboratory Outstanding Dissertation Award of 1986, IEEE 1991 Outstanding Student Branch Counselor Award, 1991 Research Award of Prof. Mustafa N. Parlar Foundation of METU, and Young Scientist Award of Scientific and Technical Research Council of Turkey in 1996.

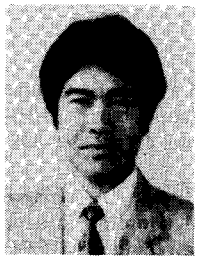

Kazuya Kobayashi was born in Tokyo, Japan, on February 28, 1955. He received the B.S., M.S., and Ph.D. degrees from Waseda University, Tokyo, Japan, in 1977, 1979, and 1982, respectively, all in electrical engineering. Since 1982, he has been with the Department of Electrical and Electronic Engineering, Chuo University, Tokyo, Japan, where he is currently a Professor. From September 1987 to August 1988, he was a Visiting Associate Professor at the Department of Electrical and Computer Engineering, University of Wisconsin-Madison, Madison, Wisconsin, USA, on leave of absence from Chuo University. His primary research interests are in the development of analytical techniques as applied to electromagnetic radiation and scattering problems. He received the Niwa Memorial Award from the Niwa Memorial Foundation, Japan, and the Shinohara Memorial Young Scientist Award from the Institute of Electronics, Information and Comunication Engineers (IEICE), Japan, both in 1983, for his contributions to the diffraction by gratings. He has contributed chapters to the books entitled, "A Course of Applied Mathematics (in Japanese)," (Corona Publishing, Tokyo, 1989), "Analysis Methods for Electromagnetic Wave Problems," (Artech House, Boston, 1990), and "Analytical and Numerical Methods in Electromagnetic Wave Theory," (Science House, Tokyo, 1993). Dr. Kobayashi is a Senior Member of the Institute of Electrical and Electronics Engineers (IEEE), and a member of the Applied Computational Electromagnetics Society (ACES), the Institute of Electrical Engineers (IEE) of Japan, and the Physical Society of Japan.

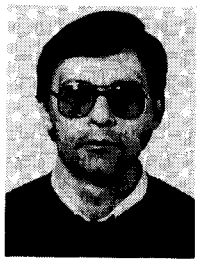

Alexander I. Nosich was born in 1953 in Kharkov, Ukraine. He graduated from the Radio Physics Department of Kharkov University in 1975. He received the Ph.D. and D.Sc. degrees in radio physics from the same university in 1979 and 1990, respectively. Since 1978, he has been on research staff of the Institute of Radiophysics and Electronics (IRE) of the Ukrainian Academy of Sciences, Kharkov. In 1992-1997, he held research fellowships and visiting professorships in Bilkent University, Turkey; Kumamoto University, Gifu University and Chuo University, Japan; University of Rennes 1, France; and Torino Polytechnical University, Italy. Currently he is with the IRE, Kharkov, as a leading scientist in the Department of Computational Electromagnetics. Since 1995, he has been on editorial board of the International Journal of Microwave and Optical Technology Letters. He is an IEEE senior member, and also a National URSI Commission B member. In 1995, he organized in Kharkov the first independent IEEE AP-S chapter in the Former Soviet Union. His research interests include free-space and open-waveguide scattering, complex mode behavior, radar cross-section modifying, and antenna simulation.